Quantum Gas of Deeply Bound Ground State Molecules

Johann G. Danzl, *et al.*

Science **321**, 1062 (2008);
DOI: 10.1126/science.1159909

Science (print ISSN 0036-8075; online ISSN 1095-9203) is published weekly, except the last week in December, by the American Association for the Advancement of Science, 1200 New York Avenue NW, Washington, DC 20005.

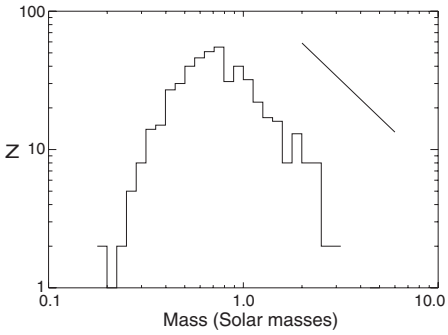

Fig. 3. Mass function of the stars formed in the simulation illustrated in Fig. 1. The stars form with masses close to 0.1 $M_\odot$ but grow quickly through gas accretion. The mass function therefore has a peak at ~0.8 $M_\odot$, above which it has a power-law form with a slope comparable to that of the Salpeter slope, illustrated by the diagonal line.

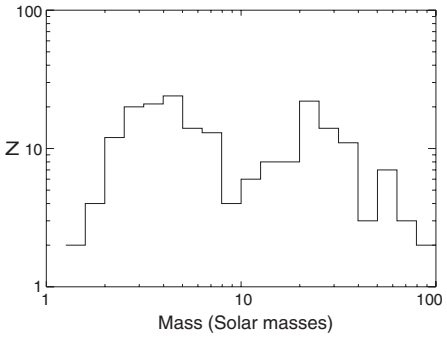

Fig. 4. Mass function of the stars formed in the simulation illustrated in Fig. 2. The mass function is extremely top-heavy and appears to have two populations of stars: one population of massive stars with masses from 10 $M_\odot$ to 100 $M_\odot$, and another with masses between 1 $M_\odot$ and 10 $M_\odot$.

involve further star formation or self-gravity–driven accretion. Assuming that all the gas would accrete directly onto the black hole on a viscous time scale (*21*) on the order of 10^7 years yields an average mass accretion rate on the order of 10^{-4} $M_\odot$/year for the 10^4 $M_\odot$ cloud and 10^{-3} $M_\odot$/year for the 10^5 $M_\odot$ cloud. This gives a maximum accretion luminosity on the order of 10^{43} ergs/s, or about 1% of the Eddington luminosity. This additional source of radiation, and that from the newly formed stars, could increase the gas temperature in the disk and thus increase the fragment masses.

Our simulations show that an infalling molecular cloud can indeed form an eccentric disk around a supermassive black hole, and that although the tidal force of the black hole will disrupt the cloud, it does not destroy the small-scale structures that seed the disk fragmentation. Furthermore, the compressional heating of the infalling gas results in the formation of a population of stars biased toward higher masses. The stellar masses depend crucially on the mass of the infalling cloud and on its impact parameter, allowing for a variety of final outcomes. The initial disk eccentricity also means that the stars can form with initial eccentricities and, if the molecular cloud is sufficiently massive, the stars that form may be extremely massive. This is therefore a viable mechanism for forming the rings of young, massive stars within ~0.1 pc of the galactic center. What is still unclear, however, is the origin of the infalling cloud and the probability of the small impact parameter that is required.

References and Notes

1. R. Genzel *et al.*, *Mon. Not. R. Astron. Soc.* **291**, 219 (1997).
2. R. Schödel *et al.*, *Nature* **419**, 694 (2002).
3. A. Ghez *et al.*, *Astrophys. J.* **620**, 744 (2005).
4. T. Paumard *et al.*, *Astrophys. J.* **643**, 1011 (2006).
5. S. Nayakshin, R. Sunyaev, *Mon. Not. R. Astron. Soc.* **364**, L23 (2005).
6. B. Elmegreen, *Astrophys. J.* **648**, 572 (2006).
7. E. S. Phinney, in *The Center of the Galaxy: Proceedings of the 136th Symposium of the IAU*, M. Morris, Ed. (Kluwer, Dordrecht, Netherlands, 1989), p. 543–553.
8. Y. Levin, A. M. Beloborodov, *Astrophys. J.* **590**, L33 (2003).
9. S. Nayakshin, J. Cuadra, *Astron. Astrophys.* **437**, 437 (2005).
10. M. A. Gürkan, F. A. Rasio, *Astrophys. J.* **628**, 236 (2005).
11. S. Nayakshin, J. Cuadra, V. Springel, *Mon. Not. R. Astron. Soc.* **379**, 21 (2007).
12. C. F. Gammie, *Astrophys. J.* **553**, 174 (2001).
13. W. K. M. Rice *et al.*, *Mon. Not. R. Astron. Soc.* **339**, 1025 (2003).
14. R. D. Alexander, M. C. Begelman, P. J. Armitage, *Astrophys. J.* **654**, 907 (2007).
15. R. D. Alexander, P. J. Armitage, J. Cuadra, M. C. Begelman, *Astrophys. J.* **674**, 927 (2008).
16. M. Wardle, F. Yusef-Zadeh, *Astrophys. J.* **683**, L37 (2008).
17. J. J. Monaghan, *Annu. Rev. Astron. Astrophys.* **30**, 543 (1992).
18. D. Stamatellos, A. P. Whitworth, T. Bisbas, S. Goodwin, *Astron. Astrophys.* **475**, 37 (2007).
19. M. R. Bate, I. A. Bonnell, N. M. Price, *Mon. Not. R. Astron. Soc.* **277**, 362 (1995).
20. See supporting material on *Science* Online.
21. The viscous time scale is the time for shearing interactions between adjacent annuli to transport mass to the central black hole.

Supporting Online Material

www.sciencemag.org/cgi/content/full/321/5892/1060/DC1
Materials and Methods
Figs. S1 to S3
References

19 May 2008; accepted 24 July 2008
10.1126/science.1160653

Quantum Gas of Deeply Bound Ground State Molecules

Johann G. Danzl,[1]* Elmar Haller,[1] Mattias Gustavsson,[1] Manfred J. Mark,[1] Russell Hart,[1] Nadia Bouloufa,[2] Olivier Dulieu,[2] Helmut Ritsch,[3] Hanns-Christoph Nägerl[1]

Molecular cooling techniques face the hurdle of dissipating translational as well as internal energy in the presence of a rich electronic, vibrational, and rotational energy spectrum. In our experiment, we create a translationally ultracold, dense quantum gas of molecules bound by more than 1000 wave numbers in the electronic ground state. Specifically, we stimulate with 80% efficiency, a two-photon transfer of molecules associated on a Feshbach resonance from a Bose-Einstein condensate of cesium atoms. In the process, the initial loose, long-range electrostatic bond of the Feshbach molecule is coherently transformed into a tight chemical bond. We demonstrate coherence of the transfer in a Ramsey-type experiment and show that the molecular sample is not heated during the transfer. Our results show that the preparation of a quantum gas of molecules in specific rovibrational states is possible and that the creation of a Bose-Einstein condensate of molecules in their rovibronic ground state is within reach.

Ultracold samples of molecules are ideally suited for fundamental studies in physics and chemistry, ranging from few-body collisional physics (*1*–*4*), ultracold chemistry (*5*), and high-resolution spectroscopy (*6*, *7*) to quantum gas preparation, molecular Bose-Einstein condensation (*8*), and quantum processing (*9*). For many of the proposed experiments, full control over the molecular wave function in specific deeply bound rovibrational states is needed. High densities are required for molecular quantum gas studies. Only in the rovibronic ground state (the lowest vibrational and rotational energy level of the electronic ground state) is collisional stability assured. However, direct molecular cooling toward high phase-space densities seems yet out of reach (*10*), whereas techniques such as Feshbach association (*11*) and photoassociation (*12*) either produce molecules exclusively in weakly bound rovibrational levels or suffer from low production rates and low state selectivity.

To produce a quantum gas of molecules in their absolute ground state, Jaksch *et al.* (*13*) proposed a scheme for homonuclear alkali molecules in which the technique of stimulated

[1]Institut für Experimentalphysik und Zentrum für Quantenphysik, Universität Innsbruck, Technikerstraße 25, 6020 Innsbruck, Austria. [2]Laboratoire Aimé Cotton, CNRS, Université Paris-Sud Bâtiment 505, 91405 Orsay Cedex, France. [3]Institut für Theoretische Physik und Zentrum für Quantenphysik, Universität Innsbruck, Technikerstraße 25, 6020 Innsbruck, Austria.

*To whom correspondence should be addressed. E-mail: johann.danzl@uibk.ac.at

two-photon transfer is repeatedly applied to molecules associated from a high-density sample of ultracold atoms. The initially very loosely bound molecules are transferred in successive steps to the rovibrational ground state of the singlet $X^1\Sigma_g^+$ molecular potential. The advantages of this scheme are that it is fully coherent, not relying on spontaneous processes, and that it involves only a very small number of intermediate levels. It promises that a ground state binding energy typically of 0.5 eV can be carried away without heating the molecular sample. It essentially preserves phase-space density, allowing the molecular sample to inherit the high initial phase-space density from the atomic sample. However, to realize this scheme, several challenges have to be met. First, there is a large difference in internuclear separation that has to be bridged: The overlap between the radial wave function of the least bound molecules and the radial wave functions of deeply bound molecular levels is extremely low, potentially leading to prohibitively low transition rates for the two-photon transitions. Second, the scheme requires the identification of suitable intermediate molecular levels while strictly avoiding parasitic excitations. Third, a large difference in binding energy has to be overcome. On a more technical side, the lasers driving the two-photon transitions at widely different wavelengths need to have extremely low relative short-term phase jitter and high long-term frequency stability to allow for coherence and reproducibility. In important experiments, Winkler *et al.* (*14*) and, recently, Ospelkaus *et al.* (*15*) demonstrated highly efficient two-photon transfer into lower-lying molecular levels starting from weakly bound dimer molecules, which were associated from ultracold atoms on a Feshbach resonance (*11*). However, the transferred molecules are still weakly bound. Their binding energy, on the order of the atomic hyperfine splitting, is $<10^{-4}$ of the binding energy of the rovibrational ground state, and wave function overlap with this state is still negligible.

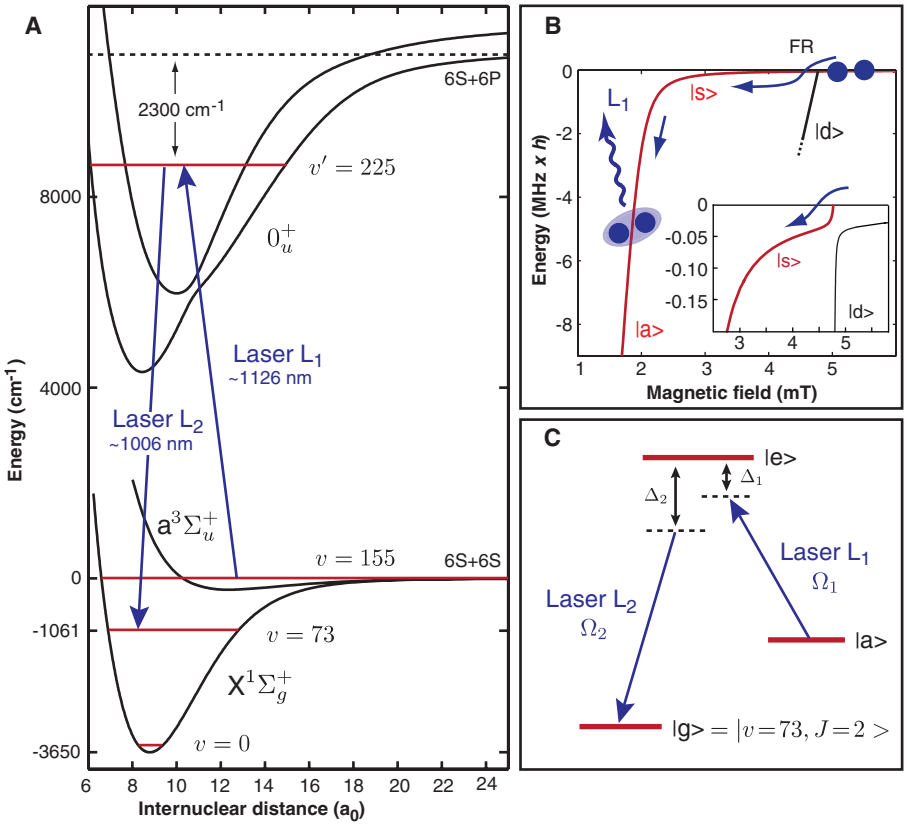

Fig. 1. (**A**) Molecular level scheme for Cs_2. Molecules in a weakly bound Feshbach level are transferred to rovibrational level $|v = 73, J = 2\rangle$ of the singlet $X^1\Sigma_g^+$ potential with a binding energy of 1061 cm^{-1} in a two-photon STIRAP process with wavelengths near 1126 and 1006 nm via the 225th level of the electronically excited $(A^1\Sigma_u^+ - b^3\Pi_u)0_u^+$ potentials. The $X^1\Sigma_g^+$ potential has about 155 vibrational levels. a_0 is the Bohr radius. (**B**) Zeeman diagram showing the energy of all relevant weakly bound molecular levels for initial Feshbach molecular state preparation (*18*). The binding energy is given with respect to the $F = 3$, $m_F = 3$ two-atom asymptote. The molecules are produced on a *d*-wave Feshbach resonance at 4.8 mT (inset) and then transferred to the weakly bound *s*-wave state $|s\rangle$ on an avoided state crossing. Further lowering of the magnetic offset field to 1.9 mT transfers the molecules from state $|s\rangle$ to state $|a\rangle$, the starting state for the STIRAP transfer. (**C**) STIRAP transfer scheme (*19*). The molecules are transferred from the initial state $|a\rangle$ to the final state $|g\rangle = |v = 73, J = 2\rangle$ by means of two overlapping laser pulses for which laser L_2 is pulsed on before L_1. The detunings and Rabi frequencies of L_i are Δ_i and Ω_i, $i = 1, 2$.

In this experiment, we demonstrate the crucial step toward full control of the molecular wave function and toward the formation of a Bose-Einstein condensate (BEC) of molecules in their rovibronic ground state by linking weakly bound molecular states with deeply bound rovibrational states. We coherently transfer an ultracold quantum gas of weakly bound cesium Feshbach molecules to the rovibrational level $|v = 73, J = 2\rangle$ of the singlet $X^1\Sigma_g^+$ potential, bound by 1061 cm^{-1} (or $h \times 31.81$ THz, where h is Planck's constant), corresponding to more than one-fourth of the binding energy of the rovibrational ground state. To achieve this result, we overcome low wave function overlap by using a suitable intermediate excited molecular state while avoiding excitation into loss channels, and we reference the transfer lasers to a frequency comb, allowing us to flexibly bridge binding-energy differences of more than 1000 cm^{-1}.

Figure 1 shows the energy of the relevant molecular and atomic states. Our experiment starts with a cigar-shaped BEC of cesium atoms in the lowest hyperfine sublevel $F = 3$, $m_F = 3$ in an optical dipole trap. For BEC production, we essentially follow the procedure detailed in (*16*). For Feshbach molecule production out of the BEC, we ramp up the offset magnetic field from the initial value of 2.1 mT to ~5.0 mT in 10 ms. We then ramp down, sweeping across a *d*-wave Feshbach resonance at 4.8 mT after ~1 ms, as shown in Fig. 1B (*17*, *18*). Our procedure [see (*17*)] gives an ultracold and dense sample of up to 11,000 molecules every 10 s at densities above 1×10^{11} cm^{-3}. For the state-transfer experiments discussed here, we do not separate the molecules from the original BEC. Upon lowering the magnetic field, the molecules are transferred from the initial state $|d\rangle$ to a still weakly bound *s*-wave molecular state $|s\rangle$ of the lowest hyperfine channel ($F_1 = 3$, $F_2 = 3$) via an avoided crossing (*18*). The index $i = 1, 2$ denotes the ith atom.

Upon further lowering the magnetic field to about 2.2 mT, the molecules enter into a closed channel *s*-wave molecular state $|a\rangle$ via a second, broad avoided crossing (*18*). This state belongs to the uppermost hyperfine channel ($F_1 = 4$, $F_2 = 4$) and thus has an effective binding energy of more than $2 \times h\nu_{Cs}$. Here, $\nu_{Cs} \approx 9.19$ GHz is the Cs clock frequency. Similar to $|s\rangle$, this state is a mixture of the $X^1\Sigma_g^+$ ground state and the lowest triplet $a^3\Sigma_u^+$ state, coupled by hyperfine interaction, and it has zero rotational angular momentum. At a field of 1.9 mT, it has a binding energy of 5 MHz $\times$ h, with respect to the $F = 3$, $m_F = 3$ two-atom asymptote (*18*). As one might expect, we find that optical transition rates as measured below are improved when using this effectively more deeply bound state as the initial state for two-photon transfer instead of state $|s\rangle$. We shut off the trap and

perform all subsequent experiments in free flight. This does not affect the particle density immediately but reduces it during the later detection procedure, which takes about 6 ms, to avoid collisions between atoms and weakly bound dimers and, hence, loss. We detect molecules in $|a\rangle$ via states $|s\rangle$ and $|d\rangle$ by first applying a magnetic field gradient for atom-molecule Stern-Gerlach separation, then reversing the magnetic field ramp, and finally dissociating them on the Feshbach resonance at 4.8 mT and imaging the resulting atoms (*17*).

Efficient two-photon transfer via the stimulated Raman adiabatic passage (STIRAP) technique (*14*, *19*) relies on a suitable choice for the excited state $|e\rangle$. In our case, this state must have singlet character so that it can be used as a transfer state to deeply bound levels of the $X^1\Sigma_g^+$ potential. In general, it must be well separated from other states, which otherwise could be off-resonantly excited. It should thus be situated far to the red of the excited $S_{1/2} + P_{1/2}$ potential asymptote to avoid the high density of excited molecular states near that asymptote. We have performed optical loss spectroscopy starting from state $|a\rangle$ in the wavelength range of 1120 to 1130 nm, ~2300 cm^{-1} to the red of the cesium D_1 line. For this measurement, we recorded the number of remaining molecules in $|a\rangle$ as a function of excitation wavelength and found two progressions of lines, which we assign to the potential curves of the mixed $(A^1\Sigma_u^+ - b^3\Pi_u)0_u^+$ excited states and to the $(1)^3\Sigma_g^+$ excited state, respectively. For the present experiments, we choose for $|e\rangle$ a level of the 0_u^+ progression that is 8879.63(1) cm^{-1} above the $F = 3$, $m_F = 3$ two-atom asymptote, corresponding to a transition wavelength of 1126.173(1) nm (Fig. 1A). We measure all wavelengths on a home-built wave meter. We identify this previously unknown level as the 225th one of the 0_u^+ system, with an uncertainty of two in the absolute numbering.

The ground state level $|g\rangle$ with vibrational quantum number $v = 73$ is well known from conventional molecular spectroscopy (*20*, *21*). However, its binding energy, as well as the binding energy of all deeply bound vibrational levels, has only been known with an uncertainty of ~±0.45 cm^{-1} before the present experiments (*21*). We search for $|g\rangle$ by simultaneously exciting the transition from $|a\rangle$ to $|e\rangle$ with laser L_1 and the one from $|e\rangle$ to $|g\rangle$ with laser L_2. The two light fields create a molecule-molecule dark state. The molecules initially in $|a\rangle$ are lost unless the second laser L_2 is on two-photon resonance, provided that the Rabi frequency Ω_2 on the second transition is $\geq\Omega_1$, the Rabi frequency on the first transition. For coherence, stability, and reproducibility, we lock both lasers to independent narrow-band optical resonators, which we reference to an optical frequency comb (*22*). The comb is not calibrated but it allows precise differential frequency measurements and provides long-term stability needed for systematic line searches (*23*). We find the resonance condition with vibrational level $v = 73$ at 1005.976(1) and 1005.982(1) nm, corresponding to rotational quantum numbers $J = 0$ and 2. Identification of J is possible because the rotational energy splitting is well known. Figure 2, A and B, shows typical molecular dark resonances when we set L_2 on resonance and step the detuning Δ_1 of L_1 near 1126.173 nm. Figure 2C shows a dark resonance involving $v = 73$, $J = 2$ using a different excited molecular state $|e'\rangle$, which is excited with L_1 near 1123.104 nm.

Figure 2, D to F, shows dark resonances involving the neighboring vibrational levels $v =$

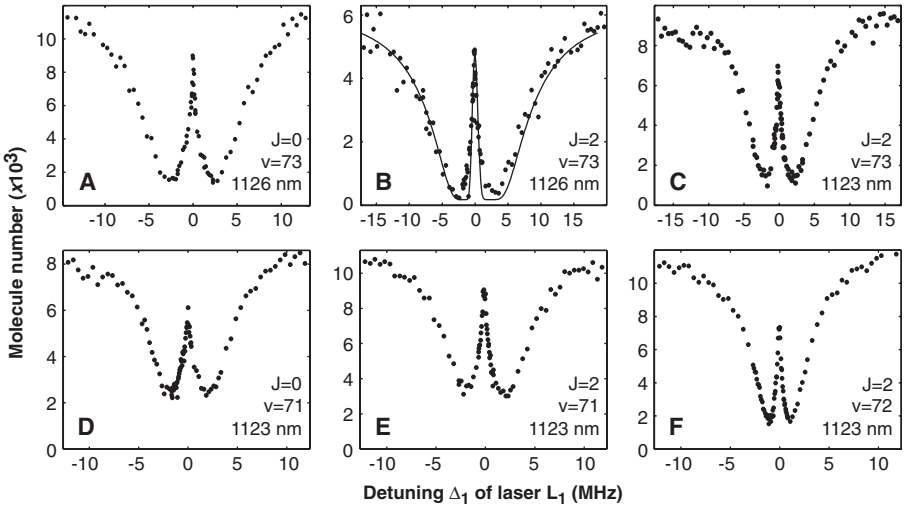

Fig. 2. Dark resonances for vibrational levels $v = 71$, 72, and 73. Laser L_2 is held on resonance while the detuning Δ_1 of L_1 is scanned. We record the number of molecules in $|a\rangle$ while both lasers are pulsed on simultaneously. (**A** to **C**) Dark resonances involving $v = 73$ for excitation with L_1 near 1126 nm into $J = 0$ and 2 and for excitation with L_1 near 1123 nm into $J = 2$, respectively. (**D** to **F**) Neighboring levels $v = 71$ and 72 for excitation near 1123 nm. The solid line in (B) is the result of a three-level model calculation matched to the data giving $\Omega_1 = 2\pi \times 2$ kHz $\sqrt{I_1/(\text{mW/cm}^2)}$ and $\Omega_2 = 2\pi \times 11$ kHz $\sqrt{I_2/(\text{mW/cm}^2)}$ for a pulse time of 5 μs at intensities of $I_1 = 4 \times 10^5$ mW/cm^2 for L_1 and $I_2 = 2 \times 10^5$ mW/cm^2 for L_2, assuming a laser linewidth of 2 kHz.

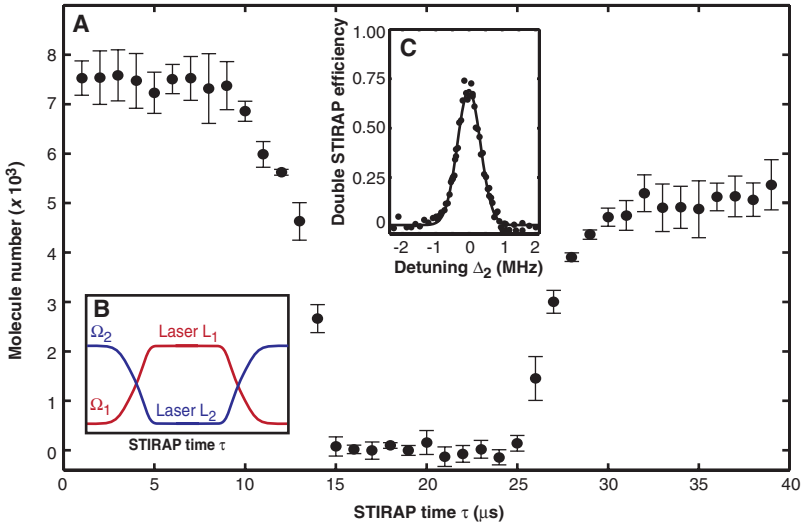

Fig. 3. STIRAP transfer from the weakly bound state $|a\rangle$ to the deeply bound state $|g\rangle = |v = 73, J = 2\rangle$ and back to $|a\rangle$. (**A**) Number of molecules in state $|a\rangle$ as a function of STIRAP time τ for $\Delta_1 \approx 0 \approx \Delta_2$. The measured pulse overlap begins at 5 μs and ends at ~15 μs. The second pulse overlap starts at 25 μs and ends at ~33 μs. (**B**) Schematic of the timing for the Rabi frequencies Ω_i, $i = 1$, 2, during the double STIRAP sequence. Laser L_1 is left on after the first STIRAP sequence to clear out any remaining population in $|a\rangle$. (**C**) Double STIRAP efficiency as a function of the detuning Δ_2 of laser L_2 for $\Delta_1 \approx 0$. The solid line is a Gaussian fit with a FWHM of 811 kHz. The peak Rabi frequencies are $\Omega_1 \approx 2\pi \times 3$ MHz and $\Omega_2 \approx 2\pi \times 6$ MHz. Error bars refer to the 1σ error in determining the particle number.

71 and 72. These $X^1\Sigma_g^+$ levels were easily found based on previously acquired Cs_2 spectra (*21*). We determine the binding energy of these levels, with respect to the atomic $F_1 = 3$, $F_2 = 3$ asymptote at zero magnetic field, to be 1060.9694(10), 1088.3101(10), and 1115.9148(10) cm^{-1} for $v = 73$, 72, and 71 with $J = 0$, respectively. The binding energy of the rovibrational ground state $v = 0$ is thus 3628.7053(14) cm^{-1}, which represents an improvement in precision of more than two orders of magnitude compared with the previous determination (*21*). Fitting the data for the dark resonances with a three-level model taking into account off-resonant excitations and laser linewidths, we determine the molecular transition strengths as given by the normalized Rabi frequencies for the transitions $|a\rangle$ to $|e\rangle$ and $|e\rangle$ to $|v = 73, J = 2\rangle$ to be $\Omega_1 = 2\pi \times 2$ kHz $\sqrt{I/(\mathrm{mW/cm^2})}$ and $\Omega_2 = 2\pi \times 11$ kHz $\sqrt{I/(\mathrm{mW/cm^2})}$, respectively. A comparison with a typical atomic transition strength of $\Omega_a = 2\pi \times 5$ MHz $\sqrt{I/(\mathrm{mW/cm^2})}$ giving $|\Omega_1/\Omega_a|^2 < 10^{-6}$ reflects the minuteness of the wave function overlap.

We are now in a position to carry out coherent transfer using the STIRAP technique. For $|g\rangle$ we choose the vibrational level with $v = 73$, $J = 2$. This level will allow us to reach the rovibrational ground state $v = 0$, $J = 0$ with a second STIRAP step in view of the selection rule $\Delta J = 0, \pm 2$. STIRAP uses a counterintuitive overlapping pulse sequence in which L_2 is pulsed on before L_1. As is well known (*19*), STIRAP relies on the existence of a dark state of the form $|D\rangle = \alpha(t)|a\rangle + \beta(t)|g\rangle$ (here, $\alpha(t)$ and $\beta(t)$ are time-dependent amplitudes with $|\alpha(t)|^2 + |\beta(t)|^2 = 1$). With sufficient adiabaticity, the function $|\alpha(t)|^2$ decreases smoothly from 1 to 0, while the function $|\beta(t)|^2$ increases smoothly from 0 to 1. The initial state $|a\rangle$ is thus rotated via $|D\rangle$ into the final state $|g\rangle$. The criterion for adiabaticity is $\tau_p\Omega^2 >> (2\pi)^2\Gamma$, where τ_p is the pulse overlap time, $\Omega \approx \Omega_1 \approx \Omega_2$ is the peak Rabi frequency during the pulse, and $\Gamma \approx 2\pi \times 4$ MHz is the (spontaneous) decay rate from the upper state $|e\rangle$, as determined from our loss measurements. This criterion is quite stringent, in particular, in view of the low wave function overlap that enters into Ω. An upper (experimental) limit for τ_p is given by the relative laser coherence time for L_1 and L_2. We choose τ_p to be ~10 μs. For detection, we apply the reverse STIRAP sequence after a waiting time $\tau_w \approx 10$ μs to transfer the molecules back into $|a\rangle$. During this time we leave laser L_1 on to assure that all possible residual population in state $|a\rangle$ is removed.

We perform double STIRAP ~3 ms after the production of the Feshbach molecules and 1 ms after shutting off the trap. Figure 3A shows the molecular population in $|a\rangle$ as a function of the STIRAP time τ, and Fig. 3B shows the timing sequence for the double-transfer scheme. For recording the time evolution of the population, we interrupt the transfer process after time τ and measure the remaining population in $|a\rangle$. The molecules in $|a\rangle$ initially disappear during the first STIRAP sequence. They are now in level $|v = 73, J = 2\rangle$ of the singlet $X^1\Sigma_g^+$ potential. Then a large fraction of them returns in the course of the reverse STIRAP sequence. For this particular measurement both lasers are on resonance. The peak Rabi frequencies are $\Omega_1 \approx 2\pi \times 3$ MHz and $\Omega_2 \approx 2\pi \times 6$ MHz. We typically obtain an overall efficiency >65% for the double-transfer process, corresponding to single-pass efficiencies >80%, assuming equal efficiencies for both passes. Figure 3C shows the double-pass efficiency as a function of detuning Δ_2 of laser L_2. Simulations for the three-level system show that the ~800-kHz full width at half maximum (FWHM) of the efficiency curve is compatible with a combination of laser power broadening and Fourier broadening. Our simulations also show that higher transfer efficiencies can be expected for an optimized STIRAP pulse sequence in which both peak Rabi frequencies are equal. Molecules not transferred by STIRAP are resonantly excited to $|e\rangle$ and then lost from our three-level system by spontaneous emission into a multitude of ground state levels.

We demonstrate coherence of the transfer process in a Ramsey-type experiment (*14*), halting the transfer process by simultaneously shutting off both lasers 12 μs into the first STIRAP sequence when a balanced superposition of $|a\rangle$ and $|g\rangle$ has been created with $|\alpha(\tau)|^2 \approx 1/2 \approx |\beta(\tau)|^2$. After a hold time τ_h we resume the STIRAP transfer, with the roles of lasers L_1 and L_2 reversed. Thus, for $\tau_h = 0$ the population will simply be rotated back into the initial state. A three-level calculation shows that the population in the initial state $|a\rangle$ is expected to oscillate at the rate of the two-photon detuning $|\Delta_2 - \Delta_1|/(2\pi)$. Figure 4A shows the initial state population for $\Delta_1 \approx 0$ and $\Delta_2 \approx 2\pi \times 113$ kHz as a function of τ_h. The population oscillates at a frequency of $|\Delta_2 - \Delta_1|/(2\pi)$, however with marked increase in phase jitter on the time scale of 30 μs. We attribute this apparent loss of phase coherence to a slow relative frequency drift of lasers L_1 and L_2, leading to a slightly different two-photon detuning from one experimental run to the next. In Fig. 4A, we have added a region indicating a frequency jitter of ±6 kHz. This value is compatible with the present long-term stability of our lasers. The frequency drift does not affect an individual STIRAP process because the transfer efficiency is very robust against laser detuning, as shown in Fig. 3C.

We now show that the molecular sample is not heated during the transfer process and is indeed in the quantum gas regime. Specifically, we measure and compare the rate of expansion of the molecular sample in state $|a\rangle$ with and without the double-transfer process. In our regime, the energy scale for expansion is usually set by the mean field of the BEC, resulting in typical expansion energies for the atoms in the range from $k_B \times 2$ nK to $k_B \times 10$ nK (where k_B is Boltzmann's constant), depending on the strength of the atomic interaction (*24*). We find that the initial magnetic field ramping excites collective motion of the BEC in the form of a breathing mode as a result of a change in the mean field potential due to a change in atomic interaction strength (*16*). The breathing is transformed into expansion of the sample when the trap is shut off. We follow the expansion by monitoring the change of the Thomas-Fermi radius r of the sample. Figure 4B shows this radius along the horizontal direction as a function of expansion time with and without STIRAP. Without STIRAP, we obtain from a linear fit an expansion rate of $dr/dt = 1.0(1)$ mm/s, corresponding to an energy of $k_B \times 14(4)$ nK. With STIRAP, the rate is $dr/dt = 0.7(1)$ mm/s, corresponding to an energy of $k_B \times 7(2)$ nK. Both values are compatible with a separate measurement of the expansion of the atomic BEC for the same magnetic field ramp. Interestingly, the rate for the case with STIRAP is lower. We speculate that STIRAP with the

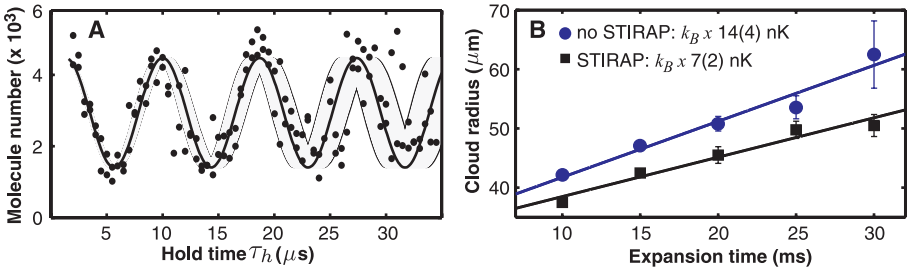

Fig. 4. (**A**) Ramsey-type experiment. The population in the initial state $|a\rangle$ oscillates as the hold time τ_h (during which both transfer lasers are off) is increased. The solid line is a sinusoidal fit to the data up to τ_h = 20 μs. Its frequency f is 115(2) kHz, in good agreement with the expected value of 113 kHz. The thin lines are borders to a region that is given by varying f by ±6 kHz, illustrating the estimated jitter in the two-photon detuning $|\Delta_2 - \Delta_1|$. (**B**) Comparison of the rate of expansion in the horizontal direction for the molecular sample without and with STIRAP transfer. The top curve (circles) shows the Thomas-Fermi radius r of the molecular sample as a function of expansion time without STIRAP. The linear fit gives a rate of expansion of dr/dt = 1.0(1) mm/s, corresponding to an energy of $k_B \times 14(4)$ nK. The bottom curve (squares) shows the expansion after double STIRAP with dr/dt = 0.7(1) mm/s, corresponding to $k_B \times 7(2)$ nK. Error bars indicate the 1σ error in the determination of the cloud radius.

tightly focused laser beams L_1 and L_2 preferentially transfers molecules in the center of the sample and is hence responsible for some selection in velocity space.

It should now be possible to add a second STIRAP step for transfer into the rovibrational ground state $v = 0$, $J = 0$. A suitable two-photon transition at readily available laser wavelengths is via the 68th excited state level of the 0_u^+ potential near 1329 nm (up) and 991 nm (down) with comparatively good wave function overlap at the level of $|\Omega/\Omega_a|^2 \approx 10^{-4}$. We expect that searching for dark resonances will be straightforward, as now all two-photon transition energies are known with an uncertainty of 10^{-3} cm^{-1}. Molecules in $v = 0$, $J = 0$ cannot further decay into a lower state upon a two-body collision, and they are thus expected to allow the formation of an intrinsically stable molecular BEC. The high speed of our STIRAP transfer will allow us to perform in situ as well as time-of-flight imaging for direct characterization of the spatial and momentum distribution of the molecular ensemble.

With our technique, any low-lying vibrational state can be coherently populated in a controlled fashion with full control over the rotational quantum number, allowing, for instance, state-specific collisional studies and high-precision molecular spectroscopy with possible implications for fundamental physics (*6*, *7*). Our procedure can be adapted to other species, in particular to heteronuclear alkali dimers such as RbCs (*25*) and KRb (*15*) for the creation of dipolar quantum gases (*26*). For heteronuclear alkali dimers, a single two-photon transfer step might suffice as a result of favorable wave function overlap (*27*). We expect that the combination of our technique with Feshbach molecule production out of a Mott-insulator state in a three-dimensional lattice (*28*) will increase the initial Feshbach molecule production efficiency, avoiding collective excitations as a result of magnetic field ramping and inhibiting collisional loss, and will provide full control over all internal and external quantum degrees of freedom of the ground state molecules.

References and Notes

1. C. Chin *et al.*, *Phys. Rev. Lett.* **94**, 123201 (2005).
2. T. Kraemer *et al.*, *Nature* **440**, 315 (2006).
3. P. Staanum, S. D. Kraft, J. Lange, R. Wester, M. Weidemüller, *Phys. Rev. Lett.* **96**, 023201 (2006).
4. N. Zahzam, T. Vogt, M. Mudrich, D. Comparat, P. Pillet, *Phys. Rev. Lett.* **96**, 023202 (2006).
5. R. V. Krems, *Int. Rev. Phys. Chem.* **24**, 99 (2005).
6. T. Zelevinsky, S. Kotochigova, J. Ye, *Phys. Rev. Lett.* **100**, 043201 (2008).
7. D. DeMille *et al.*, *Phys. Rev. Lett.* **100**, 043202 (2008).
8. M. Inguscio, W. Ketterle, C. Salomon, Eds., *Ultracold Fermi Gases, Proceedings of the International School of Physics "Enrico Fermi," Course CLXIV* (IOS Press, Amsterdam, 2008).
9. D. DeMille, *Phys. Rev. Lett.* **88**, 067901 (2002).
10. J. Doyle, B. Friedrich, R. V. Krems, F. Masnou-Seeuws, *Eur. Phys. J. D* **31**, 149 (2004).
11. T. Köhler, K. Góral, P. S. Julienne, *Rev. Mod. Phys.* **78**, 1311 (2006).
12. K. M. Jones, E. Tiesinga, P. D. Lett, P. S. Julienne, *Rev. Mod. Phys.* **78**, 483 (2006).
13. D. Jaksch, V. Venturi, J. I. Cirac, C. J. Williams, P. Zoller, *Phys. Rev. Lett.* **89**, 040402 (2002).
14. K. Winkler *et al.*, *Phys. Rev. Lett.* **98**, 043201 (2007).
15. S. Ospelkaus *et al.*, preprint available at http://arxiv.org/abs/0802.1093 (2008).
16. T. Weber, J. Herbig, M. Mark, H.-C. Nägerl, R. Grimm, *Science* **299**, 232 (2003), published online 5 December 2002; 10.1126/science.1079699.
17. J. Herbig *et al.*, *Science* **301**, 1510 (2003), published online 21 August 2003; 10.1126/science.1088876.
18. M. Mark *et al.*, *Phys. Rev. A* **76**, 042514 (2007).
19. K. Bergmann, H. Theuer, B. W. Shore, *Rev. Mod. Phys.* **70**, 1003 (1998).
20. W. Weickenmeier *et al.*, *J. Chem. Phys.* **82**, 5354 (1985).
21. C. Amiot, O. Dulieu, *J. Chem. Phys.* **117**, 5155 (2002).
22. Laser L_1 near 1126 nm and laser L_2 near 1006 nm are continuous-wave grating-stabilized tunable diode lasers with up to 26 mW and 5 mW of power at the sample position, respectively, both focused to a $1/e^2$ waist of ~25 μm for sufficiently high Rabi frequencies. We estimate the laser linewidth for both lasers to be on the order of 1 kHz. The laser beams propagate horizontally at an angle of 80° with the long axis of the BEC with vertical linear polarization. Copropagation assures that the imparted photon recoil during STIRAP is minimal, corresponding to an energy of $k_B \times 0.4$ nK, with Boltzmann's constant k_B. The beam intensity is controlled by acousto-optical modulators, allowing pulse lengths down to 1 μs.
23. The wave-meter calibration is currently not sufficient to allow absolute numbering of the frequency comb teeth.
24. T. Kraemer *et al.*, *Appl. Phys. B* **79**, 1013 (2004).
25. J. M. Sage, S. Sainis, T. Bergeman, D. DeMille, *Phys. Rev. Lett.* **94**, 203001 (2005).
26. K. Góral, L. Santos, M. Lewenstein, *Phys. Rev. Lett.* **88**, 170406 (2002).
27. W. C. Stwalley, *Eur. Phys. J. D* **31**, 221 (2004).
28. T. Volz *et al.*, *Nat. Phys.* **2**, 692 (2006).

29. We thank the team of J. Hecker Denschlag, the LevT team in our group, and T. Bergeman for very helpful discussions and M. Prevedelli for technical assistance. We are indebted to R. Grimm for generous support and gratefully acknowledge funding by the Austrian Ministry of Science and Research (Bundesministerium für Wissenschaft und Forschung) and the Austrian Science Fund (Fonds zur Förderung der wissenschaftlichen Forschung) in the form of a START prize grant and by the European Science Foundation in the framework of the EuroQUAM collective research project QuDipMol.

1 May 2008; accepted 1 July 2008
Published online 10 July 2008;
10.1126/science.1159909
Include this information when citing this paper.

Observation of Atomic Diffusion at Twin-Modified Grain Boundaries in Copper

Kuan-Chia Chen,[1]* Wen-Wei Wu,[2]* Chien-Neng Liao,[1]† Lih-Juann Chen,[1] K. N. Tu[3]

Grain boundaries affect the migration of atoms and electrons in polycrystalline solids, thus influencing many of the mechanical and electrical properties. By introducing nanometer-scale twin defects into copper grains, we show that we can change the grain-boundary structure and atomic-diffusion behavior along the boundary. Using in situ ultrahigh-vacuum and high-resolution transmission electron microscopy, we observed electromigration-induced atomic diffusion in the twin-modified grain boundaries. The triple point where a twin boundary meets a grain boundary was found to slow down grain-boundary and surface electromigration by one order of magnitude. We propose that this occurs because of the incubation time of nucleation of a new step at the triple points. The long incubation time slows down the overall rate of atomic transport.

Grain boundaries affect many physical properties of polycrystalline solids. For example, reduction of grain size is known to improve the mechanical strength of metals, governed by the Hall-Petch equation (*1*, *2*). A large-angle tilt-type grain boundary can short-circuit atomic diffusion, which has been the most serious reliability issue in Al interconnects in microelectronics technology. The atomic structure of a grain boundary is controlled by the misorientation between the two grains forming the grain boundary. Balluffi *et al.* have made bicrystals of Au thin films and varied systematically the tilt or twist angle in the bicrystals for studying the correlation between formation energy and atomic structure of grain boundaries (*3*, *4*). Generally speaking, the higher the grain-boundary misorientation angle, the higher the atomic diffusivity. Thus, by modifying the structure of a grain boundary, it should be possible to control the atomic diffusion along the grain boundary.

Lu *et al.* have synthesized a high density of nanotwins in pure Cu foils by pulsed electrodeposition (*5*). The average grain size in the Cu foils is ~400 nm, and the high-density twins have a peak at 15 nm in twin-lamella size distribution. The Cu foil shows a 10-fold improvement of the mechanical strength relative to a large-grained Cu, and the foil remains ductile but its electrical resistance did not significantly change. High mechanical strength and low electrical resistivity are desired properties for interconnecting wires in integrated circuits from the consideration of the resistive-capacitive delay, electromigration (EM), and stress migration (*6*–*8*). EM is enhanced

[1]Department of Materials Science and Engineering, National Tsing Hua University, Hsinchu 30013, Taiwan, Republic of China. [2]Department of Materials Science and Engineering, National Chiao Tung University, Hsinchu 30010, Taiwan, Republic of China. [3]Department of Materials Science and Engineering, University of California, Los Angeles, CA 90095, USA.

*These authors contributed equally to this work.
†To whom correspondence should be addressed. E-mail: cnliao@mx.nthu.edu.tw